Inorg. Chem. **2005**, *44*, 3181–3189

High-Nuclearity Mixed-Chelate Ferric Complexes from a New Family of Polynuclear Precursors

Colette Boskovic,*,† Hans U. Güdel,‡ Gaël Labat,§ Antonia Neels,§ Wolfgang Wernsdorfer,|| Boujemaa Moubaraki,⊥ and Keith S. Murray⊥

School of Chemistry, University of Melbourne, Parkville, Victoria 3010, Australia, Departement für Chemie und Biochemie, Universität Bern, Freiestrasse 3, Bern CH-3012, Switzerland, Institut de Chimie, Laboratoire de Cristallographie, Université de Neuchâtel, Avenue de Bellevaux 51, Neuchâtel CP 2, CH-2007 Switzerland, Laboratoire Louis Néel-CNRS, BP 166, 25 Avenue des Martyrs, 38042 Grenoble Cedex 9, France, and School of Chemistry, Monash University, PO Box 23, Victoria 3800, Australia

Received November 11, 2004

The syntheses, structures, and magnetochemical characterization of two novel mixed-chelate undeca- and dodecanuclear ferric complexes are reported. Preformed tri- and pentanuclear ferric complexes that possess tridentate Schiff base (L^{2-} and $(L')^{2-}$) and acetate ligands were reacted with 1,1,1-tris(hydroxymethyl)ethane (H_3thme) to afford $[Fe_{11}O_3(OH)(O_2CMe)_8(thme)_2(L)_6]$ (**1**) and $[Fe_{12}O_4(O_2CMe)_8(thme)_2(NH_2(CH_2)_2O)_2(L')_6]$ (**2**), respectively, following structural agglomeration and rearrangement associated with ligand substitution. The incorporation of more than one type of ligand that can both chelate and bridge the Fe centers gives rise to the complicated molecular structures displayed by **1** and **2**. As a result of the tripodal conformation of $thme^{3-}$, the cores of both molecules incorporate several face-shared defect $\{Fe_3O_4\}^+$ cuboidal subunits. Variable-temperature dc and ac magnetic susceptibility studies, together with low-temperature magnetization measurements, are consistent with $S = 5/2$ and $S = 0$ ground-state spins for **1** and **2**, respectively, and suggest that excited states with higher spin values lie relatively close in energy to the ground state for both species. Low-temperature micro-SQUID measurements on oriented single crystals of **1** confirm the easy-axis type magnetic anisotropy suggested by conventional SQUID magnetometry. However magnetization hysteresis is not observed down to 0.04 K, which is ascribed to rapid quantum tunneling of the magnetization associated with transverse interactions.

Introduction

High-nuclearity Fe complexes (Fe_n, $n > 10$) are of interest both as models for biological systems and as potential magnetic materials. The iron storage protein ferritin features an oxide hydroxide ferric core with up to 4500 Fe centers.[1] Polynuclear oxo- and hydroxo-bridged Fe complexes have been synthesized and studied as possible models for ferritin to provide insight into the biomineralization process associated with its formation.[2] Polynuclear Fe complexes have also been found to act as "single-molecule magnets" (SMMs),[3] displaying both slow relaxation and quantum tunneling of the magnetization at cryogenic temperatures.[4−7] The energy barrier to magnetization reversal for these complexes is of purely molecular origin, arising from a high-spin ground state

* Author to whom correspondence should be addressed. E-mail: c.boskovic@unimelb.edu.au.
† University of Melbourne.
‡ Universität Bern.
§ Université de Neuchâtel.
|| Laboratoire Louis Néel-CNRS.
⊥ Monash University.

(1) Crichton R. R. *Inorganic Biochemistry of Iron Metabolism*; Horwood: New York, 1991.
(2) (a) Gorun, S. M.; Papaefthymiou, G. C.; Frankel, R. B.; Lippard, S. J. *J. Am. Chem. Soc.* **1987**, *109*, 3337. (b) Taft, K. L.; Papaefthymiou, G. C.; Lippard, S. J. *Science* **1993**, *259*, 1302. (c) Taft, K. L.; Papaefthymiou, G. C.; Lippard, S. J. *Inorg. Chem.* **1994**, *33*, 1510. (d) Caneschi, A.; Cornia, A., Lippard, S. J.; Papaefthymiou, G. C.; Sessoli, R. *Inorg. Chim. Acta* **1996**, *243*, 295. (e) Micklitz, W.; McKee, V.; Rardin, R. L.; Pence, L. E.; Papaefthymiou, G. C.; Bott, S. G.; Lippard, S. J. *J. Am. Chem. Soc.* **1994**, *116*, 8061.
(3) Gatteschi, D.; Sessoli, R. *Angew. Chem., Int Ed.* **2003**, *42*, 268 and references therein.
(4) (a) Barra, A. L.; Caneschi, A.; Cornia, A.; De Biani, F. F.; Gatteschi, D.; Sangregorio, C.; Sessoli, R.; Sorace, L. *J. Am. Chem. Soc.* **1999**, *121*, 5302. (b) Gatteschi, D.; Sessoli, R.; Cornia, A. *Chem. Commun.* **2000**, 725. (c) Oshio, H.; Hoshino, N.; Ito, T. *J. Am. Chem. Soc.* **2000**, *122*, 12602.

10.1021/ic048411u CCC: $30.25 © 2005 American Chemical Society
Published on Web 04/05/2005

and a substantial easy-axis type magnetic anisotropy, with the magnitude of the energy barrier given by $E = S^2|D|$ for integer spin systems, where D is the axial zero-field splitting (ZFS) parameter. It has been suggested that as a result of the slow magnetic relaxation, SMMs may have potential applications in magnetic data storage, while quantum tunneling may afford the superposition of states necessary for them to act as qubits in quantum computers.[8] One approach for achieving new SMMs is to target high-nuclearity complexes, where a ferrimagnetic arrangement of the individual spins on the metal centers can afford the necessary high-spin ground state for the molecule. To date, the highest nuclearity Fe cluster that has displayed evidence for SMM behavior is an oxo- and hydroxo-bridged Fe_{19} complex with a spin ground state of $S = 33/2$.[5]

A very successful strategy for the synthesis of high-nuclearity metal complexes is the reaction of preformed lower nuclearity polynuclear complexes with chelating ligands. A family of complexes that have been widely used as starting materials in this way are the trinuclear "basic carboxylate" complexes of formula $[M_3O(O_2CR)_6X_3]^{n+}$, where M = Mn, Fe, X = H_2O, py, etc., and $n = 0$, 1.[9] These complexes are generally soluble in polar organic solvents and are very reactive toward a wide variety of chelating ligands,[10] affording complexes of varying nuclearity including Mn_{18}, Mn_{22}, and Fe_{16} species.[11,12] The agglomeration and structural rearrangement associated with the formation of these species results from a combination of the ready replacement of the terminal ligands, the chelate effect, and the basicity of the carboxylates, some of which are protonated and displaced upon coordination of a deprotonated form of the chelating ligand.

Although polynuclear metal complexes commonly contain chelating ligands, examples of such species that incorporate more than one type of chelating ligand are less common.[10b] Even rarer are metal complexes that feature multiple types of chelating ligands that simultaneously act as bridging ligands. Such complexes have the potential to manifest structures, and therefore magnetic properties, that are otherwise unobtainable. Several Ni_{10} complexes that possess β-diketonate and polyalkoxo ligands that serve in both chelating and bridging capacities have recently been reported by McInnes et al.[13] These molecules were synthesized by solvothermal methods and possess highly unusual "supertetrahedral" structures. Other work has demonstrated the efficacy of using mixed-chelate "blend" systems to access new polynuclear complexes via conventional synthetic methods under ambient conditions. For example, Perlepes et al. have recently combined di-2-pyridyl ketone with substituted catechol-based ligands in Fe chemistry to give new Fe_3 and Fe_4 complexes that incorporate both types of ligand, with each coordinating in both chelating and bridging modes.[14] These complexes clearly indicate the potential of using mixed-chelate reaction systems to obtain species with novel structures. An alternative approach to accessing mixed-chelate complexes is to react chelating ligands with preformed polynuclear complexes that already incorporate a different type of chelating ligand. The wide variety of polynuclear complexes that have been synthesized from the trinuclear "basic carboxylate" species suggests that the incorporation of replaceable carboxylate ligands in the precursor complexes may enhance the success of this approach.

As part of an investigation of the chemistry of metal complexes of ligands derived from the Schiff bases H_2L and H_2L' (Chart 1),[15] we have recently reported a new family of tri-, tetra-, and pentanuclear ferric complexes that possess these ligands together with carboxylates.[7,16] In all of these complexes the Schiff base ligands serve simultaneously in both chelating and bridging capacities. Of particular interest is one of the pentanuclear complexes, which was found to display the slow magnetization relaxation associated with SMM behavior.[7] Thus, in an attempt to synthesize new large clusters and possibly SMMs, we are targeting mixed-chelate complexes by reacting our tri-, tetra-, and pentanuclear complexes with a variety of polyalcohol-containing proli-

Chart 1. Proligands

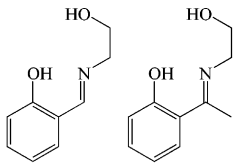

H_2L H_2L'

(5) (a) Powell, A. K.; Heath, S. L.; Gatteschi, D.; Pardi, L.; Sessoli, R.; Spina, G.; Del Giallo, F.; Pieralli, F. *J. Am. Chem. Soc.* **1995**, *117*, 2491. (b) Goodwin, J. C.; Sessoli, R.; Gatteschi, D.; Wernsdorfer, W.; Powell, A. K.; Heath, S. L. *J. Chem. Soc., Dalton Trans.* **2000**, 1835. (c) Powell, G. W.; Lancashire, H. N.; Brechin, E. K.; Collison, D.; Heath, S. L.; Mallah, T.; Wernsdorfer, W. *Angew. Chem., Int. Ed.* **2004**, *43*, 5772.

(6) Jones, L. F.; Brechin, E. K.; Collison, D.; Helliwell, M.; Mallah, T.; Piligkos, S.; Rajaraman, G.; Wernsdorfer, W. *Inorg. Chem.* **2003**, *42*, 6601.

(7) Boskovic, C.; Sieber, A.; Chaboussant, G.; Güdel, H. U.; Ensling, J.; Wernsdorfer, W.; Neels, A.; Labat, G.; Stoeckli-Evans, H.; Janssen, S. *Inorg. Chem.* **2004**, *43*, 5053.

(8) Leuenberger, M. N.; Loss, D. *Nature* **2000**, *410*, 789.

(9) Cannon, R. D.; White, R. P. *Prog. Inorg. Chem.* **1988**, *36*, 195.

(10) (a) Christou, G. *Acc. Chem. Res.* **1989**, *22*, 328. (b) Winpenny, R. E. P. *Adv. Inorg. Chem.* **2001**, *52*, 1.

(11) (a) Brechin, E. K.; Boskovic, C.; Wernsdorfer, W.; Yoo, J.; Yamaguchi, A.; Sañudo, E. C.; Concolino, T. R.; Rheingold, A. L.; Ishimoto, H.; Hendrickson, D. N.; Christou G. *J. Am. Chem. Soc.* **2002**, *124*, 9710. (b) Murugesu, M.; Raftery, J.; Wernsdorfer, W.; Christou, G.; Brechin, E. K. *Inorg. Chem.* **2004**, *43*, 4203. (c) Brechin, E. K.; Sañudo, E. C.; Wernsdorfer, W.; Boskovic, C.; Yoo, J.; Hendrickson, D. N.; Yamaguchi, A.; Ishimoto, H.; Concolino, T. E.; Rheingold, A. L.; Christou, G. *Inorg. Chem.* **2005**, *44*, 502.

(12) (a) Jones, L. F.; Batsanov, A.; Brechin, E. K.; Collison, D.; Helliwell, M.; Mallah, T.; McInnes, E. J. L.; Piligkos, S. *Angew. Chem., Int. Ed.* **2002**, *41*, 4318.

(13) (a) Shaw, R.; Tidmarsh, I. S.; Laye, R. H.; Breeze, B.; Helliwell, M.; Brechin, E. K.; Heath, S. L.; Murrie; M.; Ochsenbein, S.; Güdel H. U.; McInnes, E. J. L. *Chem. Commun.* **2004**, 1418.

(14) (a) Boudalis, A. K.; Dahan, F.; Bousseksou, A.; Tuchagues, J. P.; Perlepes, S. *Dalton Trans.* **2003**, *17*, 3411.

(15) (a) Boskovic, C.; Bircher, R.; Tregenna-Piggott, P. L. W.; Güdel, H. U.; Paulsen, C.; Wernsdorfer, W.; Barra, A. L.; Khatsko, E.; Neels, A.; Stoeckli-Evans, H. *J. Am. Chem. Soc.* **2003**, *125*, 14046. (b) Basler, R.; Boskovic, C.; Chaboussant, G.; Güdel, H. U.; Murrie, M.; Ochsenbein, S. T.; Sieber, A. *ChemPhysChem* **2003**, *4*, 910.

(16) (a) Boskovic, C.; Rusanov, E.; Stoeckli-Evans, H.; Güdel, H. U. *Inorg. Chem. Commun.* **2002**, *5*, 881. (b) Boskovic, C.; Labat, G.; Neels, A.; Güdel, H. U. *Dalton Trans.* **2003**, 3671.

gands that possess the potential to chelate and bridge simultaneously. Polyalcohol ligands were chosen due to the high affinity of ferric centers for alkoxo-based ligands. As part of this study the reaction of diol-based proligands, including catechol and 2-hydroxybenzyl alcohol, with the precursor complexes have afforded new mixed-chelate tri-, tetra-, and hexanuclear complexes that will be reported in due course. However the highest nuclearity clusters that we have obtained have featured the trianion of the triol H_3thme. The use of this particular proligand has been inspired by its successful incorporation into polynuclear complexes of V, Mo, Mn, Fe, and Ni by the groups of Zubieta, Hegetschweiler, Cornia, and Brechin.[6,12,13,17,18]

Experimental Section

Syntheses. All manipulations were performed under aerobic conditions, using materials as received. $[Fe_3(O_2CMe)_3(L)_3]$ and $[Fe_5O(OH)(O_2CMe)_4(L')_4]$ were prepared as described.[7]

$[Fe_{11}O_3(OH)(O_2CMe)_8(thme)_2(L)_6]$ (1). A solution of $[Fe_3(O_2CMe)_3(L)_3]$ (0.50 g, 0.60 mmol) and H_3thme (0.072 g, 0.60 mmol) in MeCN (40 cm^3) was stirred overnight and then filtered. The filtrate was evaporated to dryness, and the residue was redissolved in the minimum volume of MeCN (40 cm^3) and layered with two volumes of Et_2O. The product was obtained as red-brown rectangular plates, which were isolated by filtration and washed with Et_2O. Yield: 25%. A sample for crystallography was maintained in contact with the mother liquor to prevent the loss of interstitial solvent. Drying under vacuum afforded a fully desolvated sample. Anal. Calcd for $[Fe_{11}O_3(OH)(O_2CMe)_8(thme)_2(L)_6]$, $C_{80}H_{97}N_6Fe_{11}O_{38}$: C, 40.63; H, 4.13; N, 3.55. Found: C, 40.48; H, 4.03; N, 3.25. Selected IR data (cm^{-1}): 1645 (s), 1601 (m), 1546 (s), 1469 (m), 1450 (s), 1425 (s), 1339 (m), 1307 (m), 1197 (w), 1149 (w), 1127 (w), 1049 (m), 1020 (m), 927 (w), 898 (w), 875 (w), 791 (w), 757 (m), 738 (w), 640 (m), 615 (m), 560 (m), 495 (m), 460 (m), 413 (m).

$[Fe_{12}O_4(O_2CMe)_8(thme)_2(NH_2(CH_2)_2O)_2(L')_6]$ (2). A solution of $[Fe_5O(OH)(O_2CMe)_4(L')_4]$ (0.60 g, 0.47 mmol) and thme (0.057 g, 0.47 mmol) in MeCN (40 cm^3) was treated as for **1**. The product was obtained as dark red rhombus-shaped plates, which were isolated by filtration and washed with Et_2O. Yield: 30%. A sample for crystallography was maintained in contact with the mother liquor to prevent the loss of interstitial solvent. Drying under vacuum afforded a fully desolvated sample. Anal. Calcd for $[Fe_{12}O_4(O_2CMe)_8(thme)_2(NH_2(CH_2)_2O)_2(L')_6]$, $C_{90}H_{120}N_8Fe_{12}O_{40}$: C, 41.19; H, 4.61; N, 4.27. Found: C, 41.19; H, 4.57; N, 4.36. Selected IR data (cm^{-1}): 1596 (s), 1560 (s), 1470 (m), 1439 (s), 1531 (m), 1258 (w), 1232 (m), 1164 (w), 1138 (w), 1121 (w), 1105 (w), 1060 (m), 1025 (m), 931 (w), 873 (w), 849 (w), 753 (m), 708 (m), 659 (m), 630 (m), 617 (m), 604 (m), 583 (w), 525 (w), 486 (m), 461 (m), 443 (m), 421 (m).

Table 1. Crystallographic Data for **1**·Et_2O·4MeCN and **2**·2Et_2O·4MeCN

	1·Et_2O·4MeCN	**2**·2Et_2O·4MeCN
formula	$C_{92}H_{119}Fe_{11}N_{10}O_{39}$	$C_{106}H_{152}Fe_{12}N_{12}O_{42}$
fw	2603.32	2936.60
space group	$P\bar{1}$	$P\bar{1}$
a, Å	17.7648(12)	11.3921(11)
b, Å	19.763(2)	16.9719(15)
c, Å	20.5964(19)	17.5613(17)
α, deg	109.091(10)	73.557(11)
β, deg	112.105(9)	85.583(12)
γ, deg	103.271(10)	74.759(11)
V, Å^3	5794.7(9)	3142.0(5)
Z	2	1
T, K	153(2)	153(2)
λ, Å	0.710 73	0.710 73
ρ_{calc}, g cm^{-3}	1.492	1.552
μ, mm^{-1}	1.415	1.426
obsd data [$I > 2\sigma(I)$]	8851	7541
R1[a]	0.0572	0.0566
wR2[b]	0.1190[c]	0.1358[d]

[a] $R1 = \Sigma||F_o| - |F_c||/\Sigma|F_o|$. [b] $wR2 = [\Sigma w(F_o^2 - F_c^2)^2/\Sigma wF_o^4]^{1/2}$. [c] $w = 1/[\sigma^2(F_o^2) + (0.0505P)^2]$, where $P = (F_o^2 + 2F_c^2)/3$. [d] $w = 1/[\sigma^2(F_o^2) + (0.0801P)^2]$, where $P = (F_o^2 + 2F_c^2)/3$.

X-ray Crystallography. The intensity data for compounds **1**·Et_2O·4MeCN and **2**·2Et_2O·4MeCN were collected at 153 K on a Stoe image plate diffraction system using Mo Kα graphite-monochromated radiation.[19] The two compounds employed an image plate distance of 70 mm, ϕ oscillation scans 0−180°, step $\Delta\phi = 1°$, and $d_{min}-d_{max}$ 12.45−0.81 Å. The structures of all compounds were solved by direct methods using the program SHELXS-97[20] and refined using weighted full-matrix least-squares on F^2. The refinement and all further calculations were carried out using SHELXL-97.[21] Crystallographic data for **1**·Et_2O·4MeCN and **2**·2Et_2O·4MeCN are given in Table 1.

For **1**·Et_2O·4MeCN two MeCN molecules/asymmetric unit were derived from Fourier difference maps. The remaining solvent molecules were strongly disordered, and the program SQUEEZE in PLATON99[22] was used to calculate the potential solvent accessible area in the unit cell; 1306 Å^3 was calculated containing about 152 electrons. Therefore, two Et_2O and four additional MeCN molecules/unit cell were included in all further calculations. The hydroxo H atom was derived from Fourier difference maps and freely refined, while all remaining H atoms were included in calculated positions and treated as riding atoms using SHELXL-97 default parameters. All non-H atoms were refined anisotropically. An empirical absorption correction was applied using the DIFABS routine in PLATON99.

For **2**·2Et_2O·4MeCN the amine H atoms were derived from Fourier difference maps and freely refined, while all remaining H atoms were included in calculated positions and treated as riding atoms using SHELXL-97 default parameters. All non-H atoms were refined anisotropically. An empirical absorption correction was applied using the DIFABS routine in PLATON99.

Magnetic Measurements. Variable-temperature magnetic susceptibility and magnetization measurements were performed with Quantum Design MPMS-XL susceptometers, each equipped with a 5 T magnet. Data were collected on powdered dried crystals. Multiple sets of dc susceptibility data were collected with magnetic

(17) (a) Khan, M. I.; Zubieta, J. *Prog. Inorg. Chem.* **1995**, *43*, 1. (b) Hegetschweiler, K.; Schmalle, H.; Streit, H. M.; Schneider, W. *Inorg. Chem.* **1990**, *29*, 3625. (c) Cornia, A.; Gatteschi, D.; Hegetschweiler, K.; Hausherr-Primo, L.; Gramlich, V. *Inorg. Chem.* **1996**, *35*, 4414. (d) Cornia, A.; Fabretti, A. C.; Garrisi, P.; Mortalo, C.; Bonacchi, D.; Gatteschi, D.; Sessoli, R.; Sorace, L.; Wernsdorfer, W.; Barra, A. L. *Angew. Chem., Int. Ed.* **2004**, *43*, 1136.

(18) (a) Brechin, E. K.; Soler, M.; Davidson, E. J.; Hendrickson, D. N.; Parsons, S.; Christou, G. *Chem. Commun.* **2002**, 2252. (b) Brechin, E. K.; Soler, M.; Christou, G.; Helliwell, M.; Teat S. J.; Wernsdorfer, W. *Chem. Commun.* **2003**, 1276. (c) Rajamaran, G.; Murugesu, M.; Sañudo, E. C.; Soler, M.; Wernsdorfer, W.; Helliwell, M.; Muryn, C.; Raftery, J.; Teat, S. J.; Christou, G.; Brechin, E. K. *J. Am. Chem. Soc.* **2005**, *126*, 15445.

(19) *IPDS Software*; Stoe & Cie GmbH: Darmstadt, Germany, 2000.

(20) Sheldrick, G. M. SHELXS-97 Program for Crystal Structure Determination. *Acta Crystallogr.* **1990**, *A46*, 467.

(21) Sheldrick, G. M. *SHELXL-97, Program for Crystal Structure Refinement*; Universität Göttingen: Göttingen, Germany, 1999.

(22) Spek, A. L. *Acta Crystallogr.* **1990**, *A46*, C34.

fields between 0.01 and 1.0 T. Alternating current susceptibility data were recorded with an applied field of 1×10^{-4} T oscillating at three frequencies up to 1500 Hz. Pascal's constants were used to estimate the diamagnetic correction for each complex. Low-temperature magnetic measurements were performed on intact single crystals using an array of micro-SQUIDS.[23] Measurements were performed on this magnetometer in the temperature range 0.04−6K, with fields up to 1.4 T. The field can be applied in any direction by separately driving three orthogonal coils.

Other Measurements. Infrared spectra (KBr disk) were recorded on a Perkin-Elmer Spectrum One FTIR spectrometer. Elemental analyses were performed at the Ecole d'ingénieurs et d'architectes de Fribourg, Fribourg, Switzerland, and at Chemical and Microanalytical Services, Belmont, Australia.

Results

Syntheses. Overnight reaction of a solution of $[Fe_3(O_2CMe)_3(L)_3]$ in MeCN with 1 equiv of H_3thme, followed by filtration, evaporation of the filtrate to dryness, redissolution of the residue in MeCN, and layering with Et_2O, affords crystals of **1** in 25% yield after several weeks. The reaction may be written as

$$11[Fe_3(O_2CMe)_3(L)_3] + 6H_3thme + 12H_2O \rightarrow 3[Fe_{11}O_3(OH)(O_2CMe)_8(thme)_2(L)_6] + 9MeCO_2H + 15H_2L \quad (1)$$

where the oxo and hydroxo ligands in the product are derived from adventitious H_2O in the solvent, as occurs in the formation of $[Fe_5O(OH)(O_2CMe)_4(L')_4]$.[7] Varying the quantity of H_3thme in this reaction between 0.5 and 1.5 equiv also affords product **1** in similar yields.

An analogous treatment of $[Fe_5O(OH)(O_2CMe)_4(L')_4]$ with 1 equiv of H_3thme, followed by similar workup, affords crystals of **2** in 30% yield:

$$12[Fe_5O(OH)(O_2CMe)_4(L')_4] + 10H_3thme + 6H_2O \rightarrow 5[Fe_{12}O_4(O_2CMe)_8(thme)_2(NH_2(CH_2)_2O)_2(L')_6] + 8MeCO_2H + 8H_2L + 10C_8H_8O_2 \quad (2)$$

The in situ hydrolysis of $(L')^{2-}$ during formation of **2** gives rise to the $NH_2(CH_2)_2O^-$ ligands and presumably 2-hydroxyacetophenone ($C_8H_8O_2$) as a byproduct. Similar in situ hydrolyses of Schiff base ligands have been observed previously.[24] Again, varying the quantity of H_3thme in this reaction between 0.5 and 2 equiv also provides product **2** in similar yields.

It is possible to reproducibly synthesize crystalline forms of **1** and **2** in moderate yields. The formation of both species involves the loss and protonation of the acetate and Schiff base ligands of the precursor complexes in combination with deprotonation of H_3thme and addition of the $thme^{3-}$ as a ligand. Agglomeration and structural rearrangement occur over the period of several weeks that is required for crystallization of the products. It is likely that in each case a complex equilibrium exists between several species in solution, with relative solubilities determining which compound ultimately crystallizes. It is noteworthy that both **1** and **2** are minor products of these reactions and the nature of the other products is unknown. Although hydrolysis of the Schiff base ligand is observed for **2** and not for **1**, it is possible that one or more of the byproducts from the reaction that gives **1** may also contain ligands that result from a similar hydrolysis of the Schiff base.

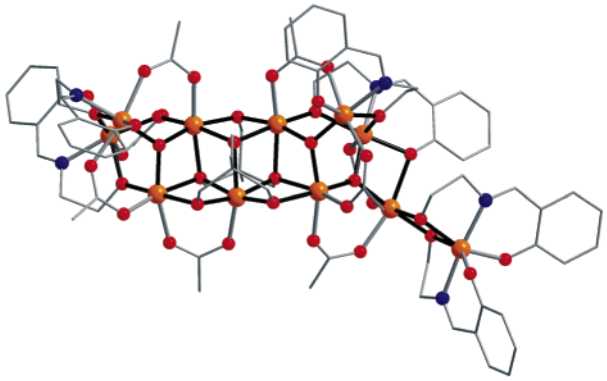

Figure 1. Structure of complex **1** in **1**·Et_2O·4MeCN.

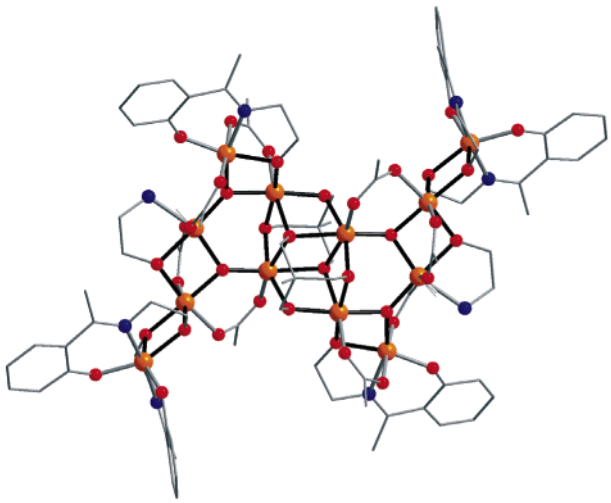

Figure 2. Structure of complex **2** in **2**·2Et_2O·4MeCN.

Structure Descriptions. Structural diagrams of complexes **1** and **2** are available in Figures 1 and 2, respectively. In addition, diagrams of the two labeled core units, together with the central fragments associated with face-sharing defect $\{Fe_3O_4\}^+$ cuboidal units, are presented in Figure 3, while diagrams of the $thme^{3-}$ binding modes present in each complex are presented in Figure 4. The most important interatomic distances and angles are available in Table 2, while a more complete listing is available in the Supporting Information.

Complex **1** (Figure 1) crystallizes in the triclinic space group $P\bar{1}$. The asymmetric unit contains the molecule of interest together with four MeCN and one Et_2O solvent molecules. Two different spatial orientations of the molecule are present within the crystal. The complex has C_1 point symmetry and possesses an $\{Fe^{III}_{11}(\mu_3\text{-}O)_6(\mu_2\text{-}O)_{11}\}^-$ core (Figure 3a), where the core O atoms are from oxo, hydroxo,

(23) (a) Wernsdorfer, W. *Adv. Chem. Phys.* **2001**, *118*, 99. (b) Wernsdorfer, W.; Chakov, N. E.; Christou, G. *Phys. Rev. B* **2004**, *70*, 132413.

(24) (a) Fenton, D. E.; Westwood, G. P.; Bashall, A.; McPartlin, M.; Scowen, I. J. *J. Chem. Soc., Dalton Trans.* **1994**, 2213. (b) Blake, A. B.; Sinn, E.; Yavari, A.; Moubaraki, B.; Murray, K. S. *Inorg. Chim. Acta* **1995**, *229*, 281.

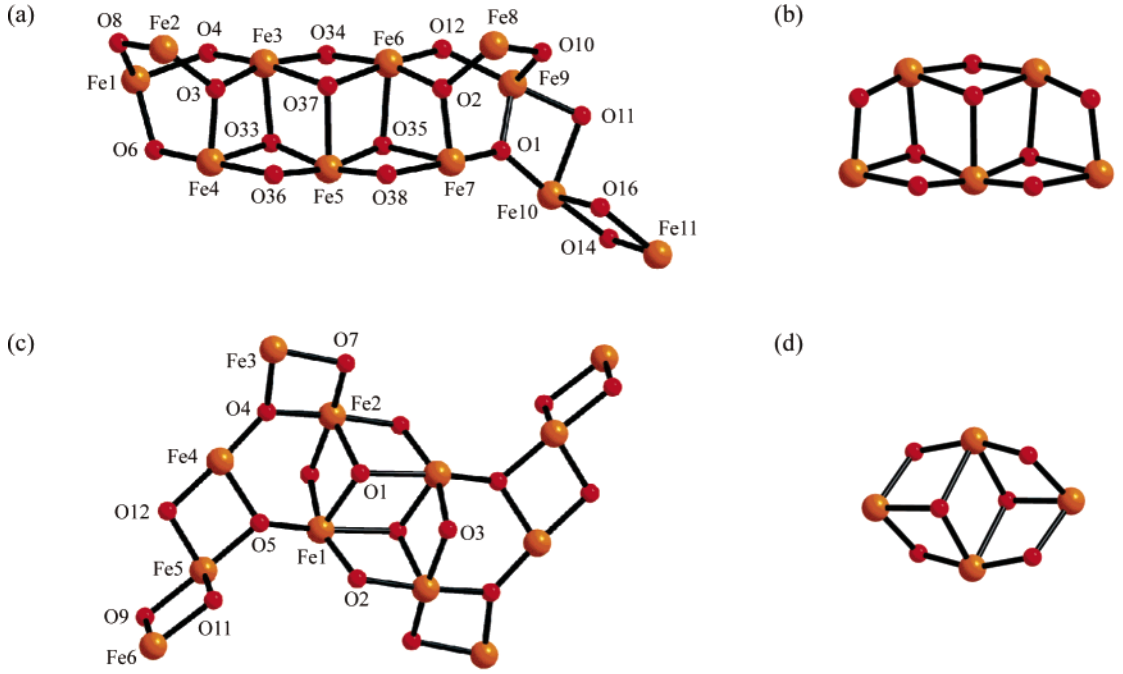

Figure 3. (a) $\{Fe_{11}O_{17}\}^{-}$ core of **1**, (b) $\{Fe_5O_8\}^{-}$ central fragment of **1**, (c) $\{Fe_{12}O_{18}\}$ core of **2**, and (d) $\{Fe_4O_6\}$ central fragment of **2**.

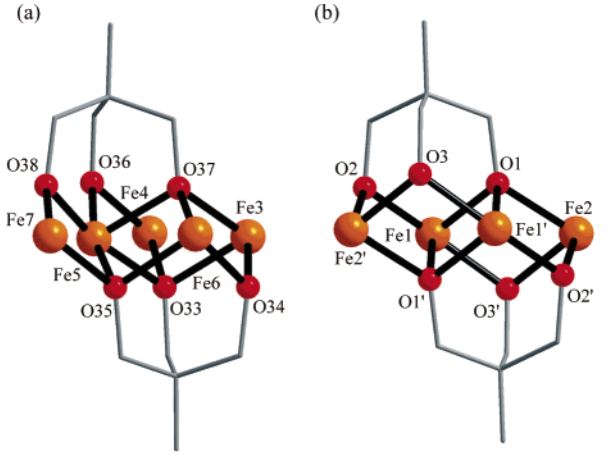

Figure 4. Structural fragments of (a) **1** and (b) **2**, showing the thme^{3-} coordination modes.

Table 2. Fe···Fe Distances (Å), Fe−O−Fe Angles (deg), and Fe−O Distances (Å) Associated with the Cores of Compounds **1**·Et_2O·4MeCN and **2**·2Et_2O·4MeCN

		1·Et_2O·4MeCN	**2**·2Et_2O·4MeCN
Fe···Fe	Fe(O)Fe	3.342(2)−3.583(2)	3.355(2)−3.446(2)
	$Fe(O)_2Fe$	3.011(2)−3.278(2)	2.931(2)−3.229(2)
Fe−O−Fe	Fe(O)Fe	118.5(2)−133.5(2)	124.7(2)−130.8(2)
	$Fe(O)_2Fe$	90.1(2)−106.7(2)	94.5(1)−107.7(2)
Fe−O		1.881(4)−2.226(4)	1.854(3)−2.243(3)

L^{2-}, or thme^{3-} ligands. The central fragment of the core contains three defect $\{Fe_3O_4\}^{+}$ cuboidal units which are face-shared in a linear arrangement to give an $\{Fe_5O_8\}^{-}$ unit (Figure 3b). Six of the eight O atoms involved in the $\{Fe_5O_8\}^{-}$ unit are from the thme^{3-} ligands (Figure 4a). The two thme^{3-} ligands coordinate in different ways, with one binding through one μ_2-O atom (O34) and two μ_3-O atoms (O33 and O35), while the other binds through two μ_2-O atoms (O36 and O38) and one μ_3-O atom (O37). The remaining μ_3-O atoms of the core (O1, O2 and O3) are from oxo ligands. Of the μ_2-O atoms, one is from the hydroxo ligand (O4), another is a phenoxo-type O atom from an L^{2-} ligand (O11), and the rest are ethoxo-type O atoms from L^{2-} ligands (O6, O8, O10, O12, O14, and O16). The peripheral ligation is completed by L^{2-} and acetate ligands. All of the L^{2-} ligands bind in the typical meridional bischelating fashion. One of the acetate ligands binds in a terminal manner, displaying an intramolecular O18···H10−O4 hydrogen bond to the hydroxo ligand with an O···O separation of 2.61 Å. The other acetate ligands bind in their commonly observed syn, syn μ_2-bridging mode. Bond valence sums are consistent with the 11 Fe^{III} centers that are required for charge balance.

Complex **2** (Figure 2) crystallizes in the triclinic space group $P\bar{1}$. The asymmetric unit contains half of the molecule of interest together with two MeCN and one Et_2O solvent molecules. In this case a single spatial orientation of the molecule is present within the crystal. The dodecanuclear complex lies on an inversion center and has C_i point symmetry. Complex **2** contains an $\{Fe^{III}_{12}(\mu_3\text{-O})_4(\mu_2\text{-O})_{14}\}$ core (Figure 3c) where the core O atoms are from oxo, $(L')^{2-}$, thme^{3-}, or $NH_2(CH_2)_2O^{-}$ ligands. The central $\{Fe_4O_6\}$ fragment of this core is composed of two face-sharing defect $\{Fe_3O_4\}^{+}$ cuboidal units (Figure 3d). All six O atoms of the $\{Fe_4O_6\}$ fragment are from thme^{3-} ligands (Figure 4b), both of which coordinate in an manner identical with that of one of the thme^{3-} ligands of **1**, binding through two μ_2-O atoms (O2 and O3) and one μ_3-O atoms (O1). The other μ_3-O atoms of the core are from oxo ligands (O4 and O5), while the μ_2-O atoms are from ethoxo-type O atoms of $(L')^{2-}$ ligands (O7, O9, and O11), or from $NH_2(CH_2)_2O^{-}$ ligands (O12). The peripheral ligation is completed by $(L')^{2-}$ and μ_2-acetate ligands binding in a manner similar to that observed in **1**, in addition to $NH_2(CH_2)_2O^{-}$ ligands. Bond valence sums are

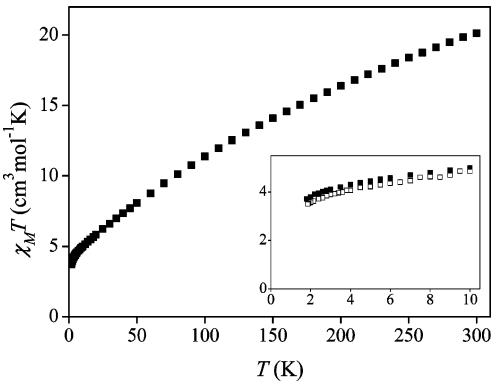

Figure 5. Plot of $\chi_M T$ vs T for **1** with $H = 0.1$ T. The inset shows the low-temperature data, and the open squares are $\chi_M' T$ data from ac susceptibility measurements with a 1×10^{-4} T field oscillating at 1000 Hz.

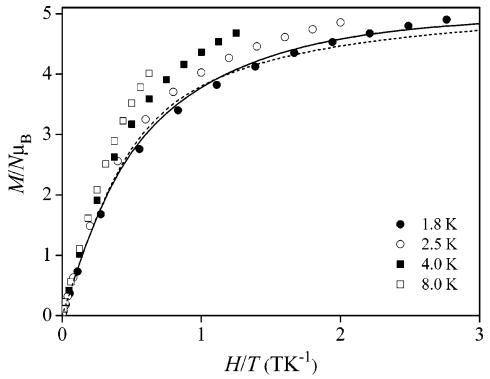

Figure 6. Plot of $M/N\mu_B$ vs H/T for **1**. The lines are calculated according to eq 3 with $S = 5/2$, $g = 2.0$, $T = 1.8$ K, and $D = -0.70$ cm^{-1} (solid line) or 1.0 cm^{-1} (dashed line).

again consistent with the 12 Fe^{III} centers that are required for charge balance.

Magnetic Measurements. Variable-temperature dc magnetic susceptibility ($T = 1.8-300$ K, $H = 0.01-1.0$ T) and variable-temperature magnetization ($T = 1.8-20$ K, $H = 0.01-5.0$ T) measurements were performed on powdered crystalline samples of complexes **1** and **2**. In addition, ac susceptibility measurements ($T = 1.8-20$ K, $H = 1 \times 10^{-4}$ T, $\nu = 100$, 1000, and 1500 Hz) were performed on **1**. The magnetic data are presented in Figures 5−8.

For **1** (Figure 5), $\chi_M T = 20$ cm^3 mol^{-1} K at 300 K, which is considerably less than the value of 48 cm^3 mol^{-1} K calculated for 11 noninteracting ferric centers with $g = 2.0$. This and the steady decrease in $\chi_M T$ as the temperature is decreased indicate substantial antiferromagnetic interactions. In particular, a gradual decrease in $\chi_M T$ is observed between 50 and 5 K and extrapolation of this to 0 K yields $\chi_M T \sim 4$ cm^3 mol^{-1} K. This is suggestive of an $S = 5/2$ ground state or an $S = 3/2$ ground state with a low-lying $S = 5/2$ excited state, as $\chi_M T$ is calculated to be 1.9 and 4.4 cm^3 mol^{-1} K for $S = 3/2$ and $S = 5/2$ systems, respectively, with $g = 2.0$. Below about 3 K, $\chi_M T$ begins to decrease more rapidly, which may be due to the presence of ZFS and/or intermolecular interactions. The high nuclearity and low symmetry of **1** preclude attempts to fit or simulate the susceptibility data, as 20 different exchange parameters would be required. To better ascertain the ground state, ac susceptibility data were obtained with a 1×10^{-4} T field (Figure 5 inset). The in-phase $\chi_M' T$ data are essentially superimposable with the dc $\chi_M T$ data (obtained with fields of 0.01−1 T), and again extrapolation to 0 K of the data above 3 K gives $\chi_M' T \sim 4$ cm^3 mol^{-1} K. This is more consistent with an $S = 5/2$ ground state than an $S = 3/2$ ground state. The very small magnetic field applied during the ac measurements should be insufficient to allow the population of excited states; thus, an $S = 5/2$ ground state seems most likely from the susceptibility data. In addition, no peak was observed in the out-of-phase χ_M'' susceptibility data down to 1.8 K.

The variable-temperature magnetization data for **1** are plotted in Figure 6 as $M/N\mu_B$ vs H/T. From the experimental data, $M/N\mu_B = 4.9$ at 1.8 K and 5 T and appears to be approaching saturation at high field, which is also consistent with an $S = 5/2$ ground state. These data deviate from the Brillouin function for $S = 5/2$, and the isotherms do not superimpose, presumably because of ZFS effects. It is possible to simulate the data obtained at 1.8 K reasonably well using the axial ZFS Hamiltonian

$$\hat{H}_{ZFS} = D(\hat{S}_z^2 - S(S+1)/3) \qquad (3)$$

(where D is the axial ZFS parameter) and assuming a well-isolated $S = 5/2$ ground state with $g = 2.0$ and $D = -0.70$ cm^{-1} (solid line, Figure 6). However, it is apparent that the experimental data exceed the calculated behavior at the highest values of H/T. This is more noticeable in the simulation of the 2.5 K data with the same parameters (not shown). At the higher temperatures of 4.0 and 8.0 K the experimental $M/N\mu_B$ data are significantly greater than the corresponding values calculated with the above parameters, and it is not possible to reproduce these data with any parameter set. These observations suggest the population of Zeeman components of low-lying excited states with $S > 5/2$. This situation is not uncommon in polynuclear ferric complexes and results from the preponderance of relatively weak antiferromagnetic pairwise interactions (vide infra) leading to a manifold of low-energy excited states.[2,5a] It should also be noted that the best simulation of the 1.8 K data with $D > 0$ requires $D = 1.0$ cm^{-1} and reproduces the experimental data less well than the simulation with $D = -0.70$ cm^{-1} (Figure 6).

To test the possibility that the magnetization data are due to $S = 3/2$ and $S = 5/2$ states that are very close in energy, values of $M/N\mu_B$ at 1.8 K and 5 T were calculated using eq 3 for energy separations between 0 and 10 cm^{-1}, with the $S = 3/2$ state above and below the $S = 5/2$ state. The observed value of 4.9 could be reproduced for an $S = 5/2$ ground state with D values between 0 and ± 0.5 cm^{-1} and an energy separation between 2 and 10 cm^{-1}. A small parameter range with an $S = 3/2$ ground state and a low-lying $S = 5/2$ excited state, between 0 and 2 cm^{-1} higher in energy, could also yield this value of $M/N\mu_B$ for $D = 0$ to ± 0.25 cm^{-1}, while the calculated $M/N\mu_B$ values decrease rapidly toward 3 for larger energy separations. Thus, these calculations also favor an $S = 5/2$ ground state for **1**.

For **2** (Figure 7), $\chi_M T = 21$ cm^3 mol^{-1} K at 300 K. This is again substantially less than the value of 53 cm^3 mol^{-1} K

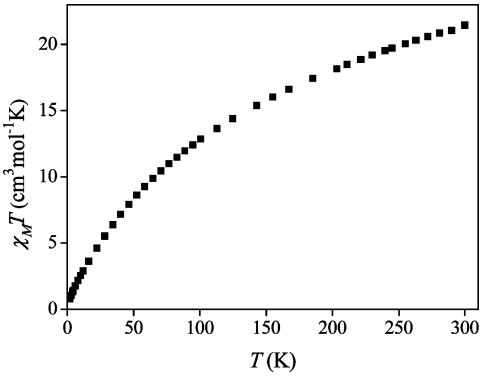

Figure 7. Plot of $\chi_M T$ vs T for **2** with $H = 1.0$ T.

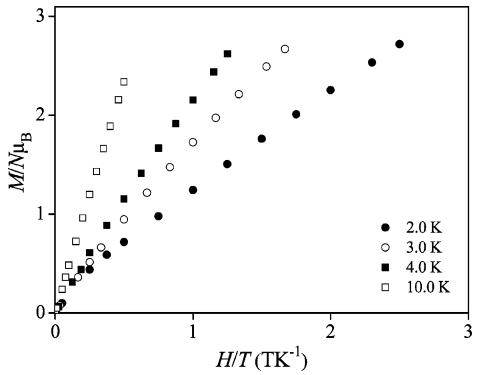

Figure 8. Plot of $M/N\mu_B$ vs H/T for **2**.

calculated for 12 noninteracting ferric centers with $g = 2.0$ and is suggestive of antiferromagnetic interactions. As the temperature is decreased, $\chi_M T$ decreases steadily to a value of 0.8 cm^3 mol^{-1} K at 2 K, consistent with a low spin, probably $S = 0$, ground state. Again the high nuclearity of **2** and the necessity to employ 9 different exchange parameters preclude attempts to fit or simulate the magnetic susceptibility data.

Variable-temperature magnetization measurements on **2** (Figure 8) reveal no sign of saturation of $M/N\mu_B$, which increases steadily as the field is increased. Increasing slopes are observed for the isotherms as the temperature is increased. This is consistent with a low-spin, probably $S = 0$, ground state and again population of Zeeman components of low-lying $S > 0$ excited states.

Micro-SQUID Measurements on Compound 1. Micro-SQUID measurements were performed on oriented single crystals of compound **1** to investigate the nature of the magnetic anisotropy. The applied field was aligned parallel to the easy axis of magnetization of the crystal using the transverse field method.[23b] The presence of such an easy axis confirms that $D < 0$ for crystals of **1**. Figure 9 presents the magnetization cycles that were obtained with the field applied parallel to the easy axis. These were measured with a sweep rate of 0.017 T s^{-1} at different temperatures in the range 0.04−6 K, with the magnetization normalized to the saturation magnetization M_S. These data can be satisfactorily reproduced across the temperature range 0.04−1 K using eq 3 with a well-isolated $S = 5/2$ ground state and $D = -0.70$ cm^{-1}; the simulations are depicted in Figure 9 as dashed lines. At higher temperatures the simulations are less

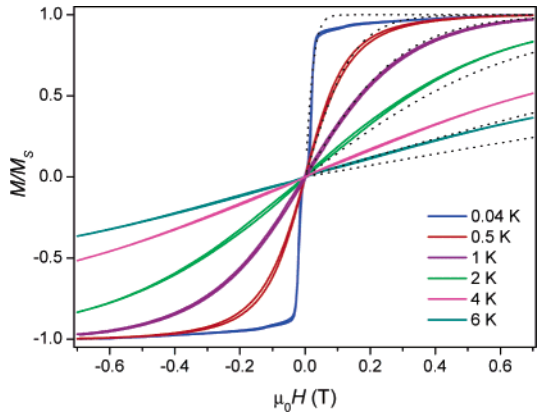

Figure 9. Field dependence of the magnetization obtained for a single crystal of **1** oriented with the field applied parallel to the easy axis at a scan rate of 0.017 T s^{-1}. The dashed lines are simulations at the given temperatures, as described in the text.

satisfactory, with M/M_S calculated to be less than the experimentally observed values. This is again consistent with the population of Zeeman components of low-lying excited states with $S > 5/2$. In contrast to the these data, when fields up to the maximum possible 1.4 T were applied to the crystal in a direction transverse to the easy axis, it was found that it was not possible to saturate the magnetization. This information can be used to give a complementary estimate of the minimum value of $|D|$. Employing the relationship[25]

$$|D| > (g\mu_B\mu_0 H_a)/(2S) \qquad (4)$$

where H_a is the maximum applied field, gives a minimum value of $|D|$ of 0.26 cm^{-1}.

It should be noted that no hysteresis due to slow relaxation of the magnetization was observed down to 0.04 K, indicating that **1** is not an SMM. In addition, close examination of the micro-SQUID magnetization data in the vicinity of $H = 0$ T reveals a sigmoidal-shaped response indicative of weak antiferromagnetic intermolecular interactions (Supporting Information). Such interactions are not uncommon in these types of polynuclear complexes, typically arising from weak intermolecular hydrogen bonds or from dipolar interactions.[15a,26]

Discussion

The ligand thme^{3-} has previously been employed in the synthesis of a number of polynuclear transition metal complexes.[6,12,13,17,18] In particular, Brechin et al. have found that reactions between the trinuclear "basic carboxylate" species $[M_3O(O_2CR)_6L_3)]^{+/0}$ (M = Mn, Fe, L = py, H_2O) and H_3thme have afforded M_n complexes (n = 8, 9, 12, 16).[12,18] In the present work, unlike the $[M_3O(O_2CR)_6L_3)]^{+/0}$ species, the tri- and pentanuclear complexes used as starting materials already possess polydentate chelating ligands and do not contain readily replaceable terminal ligands. Never-

(25) Ferbinteanu, M.; Miyasaka, H.; Wernsdorfer, W.; Nakata, K.; Sugiura, K.; Yamashita, M.; Coulon, C.; Clérac, R. *J. Am. Chem. Soc.* **2005**, *127*, 3090.
(26) Affronte, M.; Sessoli, R.; Gatteschi, D.; Wernsdorfer, W.; Lasjaunias, J. C.; Heath, S. L.; Powell, A. K.; Fort, A.; Rettori, A. J. *Phys. Chem. Solids* **2004**, *65*, 745.

theless, the formation of multiple chelate rings associated with coordinated thme^{3-}, combined with the basicity of the acetate ligands of the precursor complexes, provides the driving force for the formation of products of higher nuclearity than the tri- and pentanuclear starting materials.

A search of the Cambridge Crystallographic Database reveals that the structures of **1** and **2** are unknown for any metal complexes. The cores of **1** and **2** incorporate three and two face-shared defect $\{Fe_3O_4\}^+$ cuboidal units, respectively (Figure 3), where six of the oxygen atoms in these units are from the thme^{3-} ligands (Figure 4). The tripodal conformation of thme^{3-} ensures that fragments comprised of such face-shared defect cuboidal units are commonly observed in complexes that contain it,[6,13,17,18] although, as seen in complexes **1** and **2**, this can result from multiple possible binding modes, with each of the three O atoms capable of binding in μ_2 or μ_3 modes. Thus, thme^{3-} has been observed to bind in polynuclear metal complexes through three μ_3-O atoms, two μ_3- and one μ_2-O atoms, one μ_3- and two μ_2-O atoms, and three μ_2-O atoms. Comparison of **1** and **2** with a recently reported family of Mn_n ($n = 6$, 6, 7, 8 and 12) "rods" that contain thme^{3-} is of particular interest, as the cores of the Mn complexes contain 4, 2, 3, 4, and 8 face-shared defect cuboidal units, respectively, revealing how the overall structures can be built up by successive addition of these units.[18b,18c] Although the core units of these Mn complexes differ from those of **1** and **2**, the structural relationship is clearly evident. Structural similarities between fragments of the cores of **1** and **2** and those of the Fe_{17} and Fe_{19} complexes of Powell and Heath et al. are also evident,[5] with the Fe_{17} and Fe_{19} complexes containing central units that are essentially comprised of six $\{Fe_3O_4\}^+$ face-shared defect cuboidal units arranged in a circle.

The experimental evidence is consistent with $S = 5/2$ and $S = 0$ ground-state spins for **1** and **2**, respectively, with low-lying excited states with larger S values present for each compound. These S values arise from the combination of the individual exchange interactions between pairs of Fe centers. These interactions are mediated through O atom bridges which are comprised of oxo-, hydroxo-, alkoxo-, and phenoxo-type bridges in **1** and oxo- and alkoxo-type bridges in **2**, in addition to acetate bridges. Pairs of Fe centers are linked by one or two O atom bridges in both complexes, and the relevant interatomic distances and angles are provided in Table 2. Pairwise exchange interactions mediated through similar bridges in other complexes are nearly always antiferromagnetic.[2,27] The complete computational analysis that would be required to rationalize the ground states determined for **1** and **2** is beyond the scope of this study. However, to provide some insight into the coupling that is present, the empirical relationship

$$-J = 2 \times 10^7(0.2 - \cos\varphi + \cos^2\varphi)\exp(-7r) \qquad (5)$$

recently reported by Christou et al. may be applied. This relationship correlates the coupling constant (J) with the Fe−O−Fe angle (φ) and the Fe···Fe distance (r) for interactions between pairs of Fe^{III} centers bridged by oxo, hydroxo, and alkoxo ligands in Fe_n complexes of nuclearity greater than two.[28] Equation 5 assumes the exchange Hamiltonian of the form

$$\hat{H}_{ex} = -2J\,\mathbf{S}_1\cdot\mathbf{S}_2 \qquad (6)$$

and applies to pairs of Fe centers that are bridged by one or more of the above ligands. When more than one ligand is present, the parameters associated with the shortest Fe−O bridge are employed. For the present complexes, the J values calculated for pairs of Fe centers using eq 5 vary from -4 to -40 cm^{-1} for **1** and from -2 to -44 cm^{-1} for **2** (Supporting Information). It must be emphasized that these values are by no means definitively determined and have been calculated merely to provide insight into two complex systems. The large number of pairwise antiferromagnetic interactions of comparable magnitude in both **1** and **2** preclude the proposition of a simple "spin up" and "spin down" argument to explain the observed ground states, and it likely that a complex spin arrangement exists in both species. This is particularly the case given that many of the antiferromagnetic pairwise interactions are essentially competing within the triangular units that make up the cores of both **1** and **2.** Moreover such a situation typically leads to a manifold of energy levels that are very close in energy and therefore to the ready population of low-lying excited states, as is suggested by the magnetic data obtained for **1** and **2**.[2,5a]

It is of some value to consider the discrete tetranuclear ferric clusters that contain an $\{Fe4O_6\}$ core that is isostructural to the $\{Fe_4O_6\}$ central unit of **2**.[29] The interatomic distances and angles evident in this subunit of **2** are comparable to those of the tetranuclear complexes. The magnetic susceptibility data for one of these tetranuclear complexes was fit to the appropriate theoretical expression, indicating weakly antiferromagnetic pairwise interactions of the order of -10 cm^{-1}, which lead to an overall $S = 0$ ground state for the complex.[29b] This is in agreement with the J values calculated for the corresponding subunit of **2** using eq 5, which vary from -2.7 to -9.9 cm^{-1}. Assuming that the total spin of the analogous $\{Fe_4O_6\}$ central subunit of **2** is $S = 0$, the symmetry-imposed antiparallel arrangement of the total spins of the two peripheral subunits of the centrosymmetric complex will inevitably lead to an $S = 0$ ground state for the whole molecule.

Micro-SQUID measurements performed on oriented single crystals of **1** confirm the presence of an easy axis in the crystal. The assumption of a strictly axial system with a well-isolated $S = 5/2$ ground state and $D = -0.70$ cm^{-1} provides a satisfactory simulation of the magnetization data obtained on a dried powder sample of **1** with a conventional SQUID at 1.8 K and of the micro-SQUID data obtained on an

(27) (a) Kurtz, D. M. *Chem. Rev.* **1990**, *90*, 585 and references therein. (b) Neves, A.; de Brito, M. A.; Vencato, I.; Drago, V.; Griesar, K.; Haase, W. *Inorg. Chem.* **1996**, *35*, 2360. (c) Ménage, S.; Que, L., Jr. *Inorg. Chem.* **1990**, *29*, 4293.

(28) Canada-Vilalta, C.; O'Brien, T. A.; Brechin, E. K.; Pink, M.; Davidson, E. R.; Christou, G. *Inorg. Chem.* **2004**, *43*, 5505.

(29) (a) Li, H.; Zhong, Z. J.; Chen, W.; You, X. Z. *J. Chem. Soc., Dalton Trans.* **1997**, 463. (b) Glaser, T.; Lügger, T. *Inorg. Chim. Acta* **2002**, *337*, 103.

oriented single crystal of **1** at $T < 2$ K. At higher temperatures the population of Zeeman components of low-lying excited states with $S > 5/2$ prevents simulation of the experimental data using this simple model. If **1** is a SMM with $S = 5/2$ and $D = -0.70$ cm^{-1}, a theoretical energy barrier to magnetization relaxation may be calculated as $(S^2 - 1/4)|D| = 4.2$ cm^{-1} and the observation of slow magnetic relaxation might be anticipated at sufficiently low temperature. However, it is important to consider that the assumption of a strictly axial system is a priori an approximation. Indeed, the lack of hysteresis in the micro-SQUID data for **1** is likely due to rapid quantum tunneling of the magnetization associated with transverse interactions. Some of us have recently reported a detailed investigation of a Ni_4 complex with $S = 4$ and $D = -0.9$ cm^{-1}, with a calculated energy barrier to magnetization reversal of $S^2|D| = 14.4$ cm^{-1}.[30] Although slow magnetization relaxation might be expected for a molecule with a calculated energy barrier of this size, significant transverse interactions result in rapid quantum tunneling of the magnetization, preventing the observation of hysteresis down to 0.04 K. Similar rapid quantum tunneling was reported for an Fe_{11} complex with $S = 11/2$ and $D = -0.46$ cm^{-1} (for a noninteger spin system the energy barrier is given by $(S^2 - 1/4)|D| = 13.8$ cm^{-1}) and was also ascribed to the effect of transverse interactions.[6]

The origin of the molecular magnetic anisotropy in polynuclear metal complexes is due to a combination of the single-ion and spin−spin anisotropies. Even though high-spin Fe^{III} has an orbital singlet ^6S ground term for the free ion, admixture with excited states of lower spin multiplicity is allowed and ZFS may be observed for the $S = 5/2$ ground state. In addition, it has been demonstrated that spin−spin interactions in antiferromagnetically coupled polynuclear ferric complexes can provide an easy-axis type contribution to the molecular magnetic anisotropy.[31] Nevertheless, estimates of D for polynuclear ferric complexes are rarely more negative than -0.3 cm^{-1}.[3−7] Thus, although there is good evidence for $D < 0$ for **1**, the precise magnitude of D is uncertain and its elucidation would require the inclusion of rhombic and possibly higher order terms in the ZFS Hamiltonian.

(30) Sieber, A.; Boskovic, C.; Bircher, R.; Waldmann, O.; Ochsenbein, S. T.; Güdel, H. U.; Kirchner, N.; van Slageren, J.; Wernsdorfer, W.; Neels, A.; Stoeckli-Evans, H.; Janssen, S.; Juranyi, F.; Mutka, H. Accepted for publication.

Conclusions

A new family of tri- and pentanuclear ferric complexes that incorporate tridentate Schiff base ligands together with acetate ligands have proved to be useful precursors for the synthesis of new high-nuclearity ferric complexes. The reaction of these precursors with the polyalcohol proligand H_3thme has afforded novel undeca- and dodecanuclear mixed-chelate species. In these complexes the different chelating ligands also bind in a bridging manner, which gives rise to novel structures that would otherwise be unobtainable. This suggests that other polynuclear metal complexes that contain chelating and carboxylate ligands may also prove to be useful starting materials for the synthesis of novel complexes, particularly upon reaction with additional chelating ligands that can also simultaneously bridge the metal centers. Magnetic characterization reveals $S = 5/2$ and $S = 0$ ground states for the undeca- and dodecanuclear complexes, respectively, with excited states with larger S values lying close in energy to the ground state for both complexes.

Acknowledgment. We thank Mr. Kevin Berry, Westernport Secondary College, Victoria, Australia, for helpful discussions. A part of this work was supported by the Swiss National Science Foundation.

Supporting Information Available: X-ray crystallographic files in CIF format for **1**·Et_2O·4MeCN and **2**·2Et_2O·4MeCN, tables of selected interatomic distances and angles for **1**·Et_2O·4MeCN and **2**·2Et_2O·4MeCN, a table of calculated J values for Fe pairs in compounds **1**·Et_2O·4MeCN and **2**·2Et_2O·4MeCN, and a figure of the low-field region of the field dependence of the magnetization obtained for a single crystal of **1** oriented with the field applied parallel to the easy axis. This material is available free of charge via the Internet at http://pubs.acs.org.

IC048411U

(31) Gatteschi, D.; Sessoli, R.; Cornia, A. *Chem. Commun.* **2000**, 725.